Mechanics & Industry **21**, 617 (2020)
© AFM, EDP Sciences 2020
https://doi.org/10.1051/meca/2020089

Mechanics & Industry

Available online at:
www.mechanics-industry.org

Regular Article

Resonance track-and-dwell testing for crack length measurement on 304L stainless steel

Christophe Gautrelet[1,*], Leila Khalij[1], and Marcela Rodrigues Machado[2]

[1] Normandie Université, Laboratoire de Mécanique de Normandie (LMN)/INSA ROUEN Normandie
[2] Department of Mechanical Engineering, University of Brasilia, 70910-900, Brasilia, Brazil, France

Received: 11 May 2020 / Accepted: 16 November 2020

Abstract. Experimental vibration-fatigue tests were conducted with sine resonance track-and-dwell (SRTD) tool by using an electrodynamic shaker on specimens made of 304L stainless steel. Due to cyclic fatigue resulting in stiffness loss, it can be found that the resonant frequency decreases when the specimen experiences substantial crack growth, especially for out-of-plane bending mode. The specimens were equipped by a crack propagation gauge (CPG) to monitor the crack growth. However, the presence of crack was detected late by these gauges. The deviation of the resonance frequency was therefore analysed from the time response measurements, and the results were confronted to the CPG measurements to conclude on the validity of the detection threshold provided by the literature.

Keywords: Vibration-based bending tests / high cycle fatigue / resonant frequency deviation / fatigue crack growth / sine resonance track-and-dwell (SRTD)

1 Introduction

Normandy region is concerned about a lot of industrial risks (fire, explosion, toxic dispersion). Dreal Normandie has identified 86 Seveso classified industrial sites and more than 10 000 km of piping (for hydrocarbon transport, chemical products, high-pressure gas, ...). Since January 2000, the ARIA database (Analysis, Research and Information on Accidents) has identified in France ninety-five accidents due to vibrations, eleven of which were reported in Normandy. For example, in Grand Quevilly town (in the Normandy region), a high-pressure water vapour pipe in a fertiliser factory had burst to lead to the projection of a 40 kg block of steel. The block crossed the ammonia confinement space 25 m further, without causing any damage, and then landed 230 m away in a parking area for ammonia tanker cars awaiting shipment, which fortunately happened to be empty that day. This accident could have had much more severe consequences, especially if it had caused a chain reaction by a cumulative effect. Great Britain, Health & Safety Executive [1] recognises that vibration-induced fatigue is the second cause of hydrocarbon releases because of catastrophic failures in piping and especially in small connections. Therefore, vibration-induced fatigue failure represents a severe risk to the environment, workers and people.

Austenitic stainless steel is widely used in several industries, especially for piping in the nuclear reactors and chemistry or petrochemistry [2]. However, despite an extensive database, extant literature contains few studies that explore the behaviour in vibration-fatigue of the stainless-steel material. Mittal et al. [3] highlighted the effect of vibration of the austenitic stainless-steel piping on the fatigue life by comparing experiments under vibration and cyclic loading. The authors showed a reduction in the fatigue initiation life by 20–35% for notched specimens subjected to vibration prior to the cyclic loading in the Low Cycle Fatigue regime. Vibration-fatigue analysis implies the fatigue analysis when the structure vibrates under resonance condition [4]. Therefore, one way to carry out vibration fatigue tests is to use an electrodynamic shaker, employed to perform a high number of cycles in a short period. Crack propagation is a small portion of total life under high-cycle tensile fatigue [5–7], the bending mode excited by the vibration-based fatigue machine allows differentiating the crack growth stages by exploiting resonance vibration [8]. But it was necessary to establish an approach to determine these stages since it is not possible to carry out this analysis during the tests.

Research efforts helped to develop non-destructive monitoring techniques to track crack initiation and growth [8,9], which is often relatively expensive. Other procedures

* e-mail: christophe.gautrelet@insa-rouen.fr

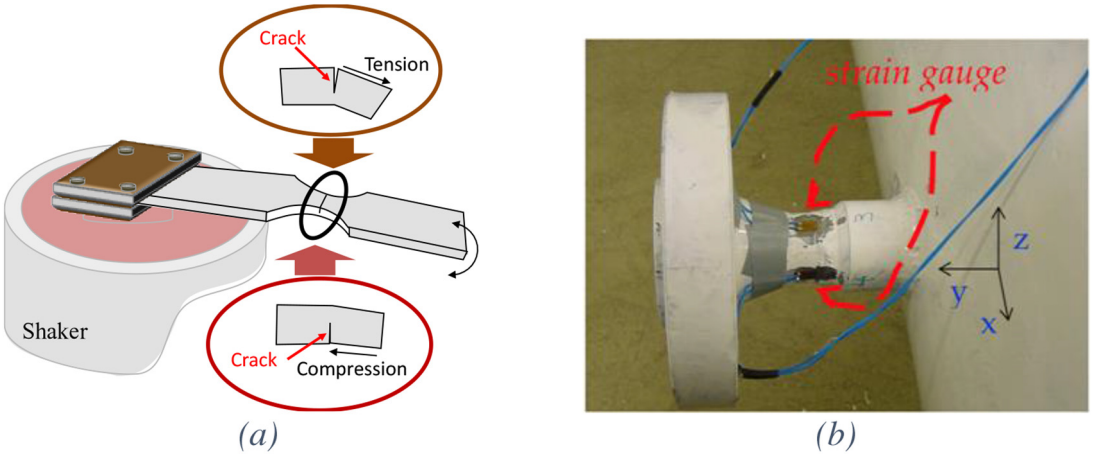

Fig. 1. (a) Schematic representation of the deflection in bending mode and (b) an example of bending measurement on a piping element with a strain gauge (Source [18] with permission of Efterklang^{TM} part of AFRY).

[10–12] require periodical pauses in the tests to inspect the specimen and measure the crack length or to identify resonant frequency. It involves replacing the specimen for the next fatigue tests, which implies a variation on the experimental conditions. Furthermore, the establishment of a minimum crack size being complex, a crack with a noticeable length can, therefore, be present and grow in the specimen before the measuring system detects it.

The literature on vibration-fatigue testing provides a large number of investigations to find a failure criterion that correlates crack detection with a significant reduction in the resonant frequency (or natural frequency). As pointed out by Salawu [13], this reduction should be set at 5% so that damage can be detected with confidence [14]. Researchers such as Xu et al. [15,16] have also adopted this threshold. The authors have selected the 5% failure criterion based on the relation between the natural frequency drop and crack size to study the fatigue properties of Ti-6Al-4V annular discs. Other researchers such as Hu et al. [17] showed that the reduction of natural frequency is less than 5% and improved this value by choosing the threshold at 2.8%. They developed a nonlinear model based on the change of natural frequency to predict the fatigue damage of 2024-T3 aluminium plate. George et al. [5] set the arbitrary value at 0.5% to test 6061-T6 aluminium and Ti-6Al-4V plate specimens. Bruns et al. [6] set 0.1% as a significant change of the resonant frequency.

In this work, crack propagation gauges and an automatic phase sine resonance track-and-dwell (SRTD) tests were used for monitoring the crack growth on 304L stainless steel plate specimens. The confrontation of the results highlighted that the 5% threshold produces a noticeable crack length which can be associated with a critical length for the geometry and the material studied.

2 Materials and methods

2.1 Equipment for HCF testing

When a pipe vibrates, the top of this component is alternately in tension and compression, causing cyclic stresses, which can potentially damage the pipe by fatigue (see Fig. 1). To model this behaviour, fatigue tests were conducted on a fatigue testing machine that generated a plate bending mode using an electrodynamic shaker (Fig. 3). The specimens were machined from 2 mm thickness 304L stainless steel plate, which may represent a small part of the piping. A reduced section was designed to localise the crack initiation far from the clamp (Fig. 2a). The width of this section was chosen identical to the width of the gauge used for monitoring the crack propagation. The numerical model (Fig. 2b and 2c) with the mechanical properties presented in Table 1 leads to a resonant frequency close to 310 Hz.

One end of the specimen (hatched part in Fig. 2a) was clamped at the head of the electrodynamic shaker, the other being left free. The fixture developed in the laboratory ensures a maximal pressure on the part of the specimen [19] to avoid transversal movement during the test. The tightening control was done with a torque wrench, and a template was used to position the specimen repeatedly.

Each of eight tests was performed with acceleration-control using the same instrumentation in the same setup, four specimens being additionally equipped by crack propagation gauges (CPG). The instrumentation, schematically depicted in Figure 3, consists of:

- Two accelerometers: a PCB 333A30 is fixed on the head of the shaker to ensure the closed-loop control, a Dytran 3225F3 is fixed just above the reduced section of the specimen (free tip) to determine the transmissibility. The second accelerometer is chosen as light as possible (0.6gr) to avoid modification of the dynamic response of the specimen.
- Strain gauges (HBM 1LY15-1.5/350) glued on the useful surface to measure the strain levels and ensure the same response for all specimens. The system linearity, given by the relationship between the excitation and the response of the specimen, has been verified in a similar way to the work referenced [20].
- Crack propagation gauges HBM RDS22 glued on the useful surface to follow the crack growth. The CPG (Fig. 4) is an assembly of 50 identical links of resistance in

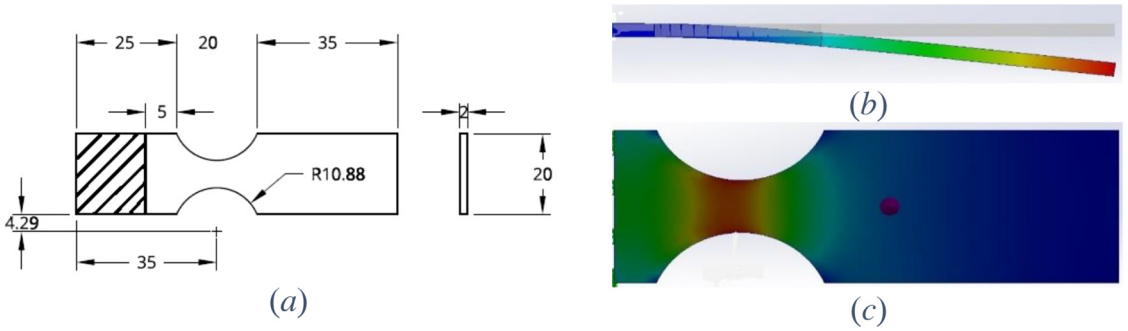

Fig. 2. (a) Dimension of the specimen (in mm), (b) vertical displacement and (c) longitudinal strain distribution (the red zone shows the uniformity of strain distribution) associated with modal analysis using a finite element model.

Table 1. Mechanical properties of the 304L stainless steel.

Young modulus (GPa)	Yield strength at 0.2% (MPa)	Density (kg/m^3)	Poisson coefficient
200	200	7900	0.3

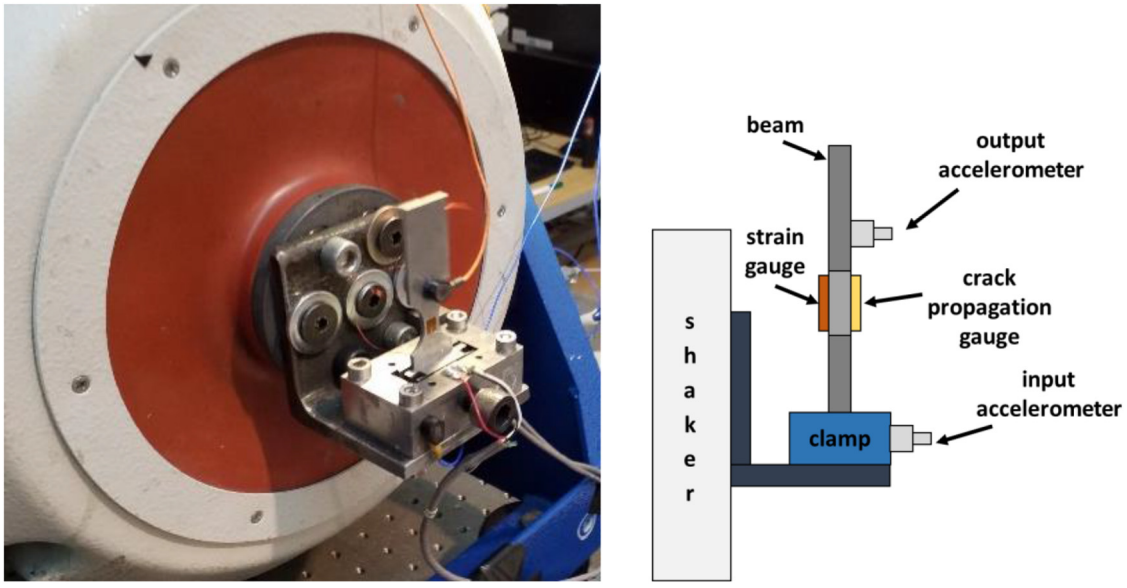

Fig. 3. Fatigue testing system and detail of instrumentation.

parallel. The links should break with the crack growth and the total resistance value of this sensor increase. From Table 2, the crack length can be deduced from the values of the resistance against broken links (Fig. 5). The measurement grid is narrower the sensor width; the first link is therefore at 1 mm from the edge of the reduced section.

It was assumed that the crack starts on one edge of the reduced section and grows in the transverse direction (see Fig. 1a), almost across the width of the reduced section.

2.2 Experimental procedure

Experimental fatigue tests were performed with the Sine Resonance Track and Dwell (SRTD) tool. The SRTD algorithm used by the control software selects and automatically tracks the phase value to produce the maximum transmissibility magnitude at a particular resonance [21]. For each of the eight specimens tested, the initial value of the excitation frequency was selected near the numerical resonant frequency value to conduct the system to track the phase at 90° since it allows the excitation frequency to match to the change in resonant frequency. This resonant frequency was then recorded (see Fig. 8) until the test stopped corresponding to a phase error, reaching a value higher than 30°. However, the specimens did not experience complete separation at the end of the test [6,15]. The number of cycles at failure was therefore reached from time and frequency values cumulated during the test until the end.

The initial resonant frequencies values, denoted f_r^0, providing by the SRTD tool for uncracked specimens are presented in Table 3.

Table 2. Characteristics of the CPG.

R per link (Ω)	Dimensions of the grid (mm)		Dimensions of the sensor (mm)		Distance between the links (mm)	Number of links
	Length a	Width b	Length c	Width d		
44	22	5	27.8	6.8	0.1	50

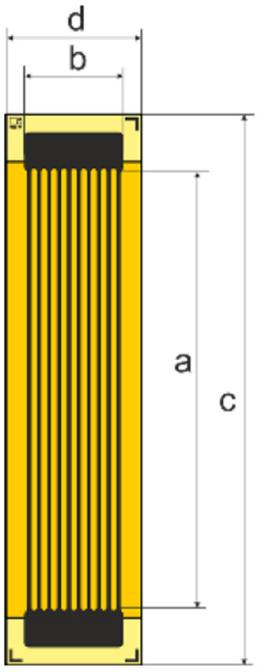

Fig. 4. RDS22 HBM.

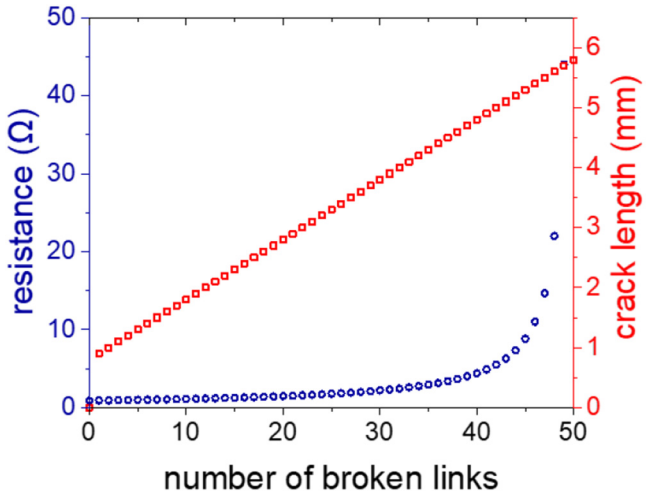

Fig. 5. Theoretical results from the HBM RDS22 CPG.

Table 3. First measurements on the specimens tested.

Id specimen	Strain amplitude (μm/m)	f_r^0 (Hz)
Inox7	**1332**	**318.1**
Inox8	**1431**	**319.5**
Inox11	1147	314.4
Inox12	1292	309.4
Inox14	1222	314.2
Inox15	1357	315.2
Inox17	**1312**	**317.4**
Inox20	**1455**	**317.2**
Average	1318.5 ± 50.9	$315{,}7 \pm 1.6$

The specimens equipped by CPG are highlighted in bold.

The strain values corresponding to the amplitudes extracted from the strain gauge measures are also added in this table. These values gave the response levels for each specimen and highlighted the relatively low disparity, probably due to the machining mode (water jet cutting system). The time signals of the two accelerometers, the strain gauge and CPG were stored during the fatigue tests. Figure 6 exhibits an example of the time signal of the input acceleration measured for *inox20.*

3 Results and discussion

The time signals were recorded with 4800 samples per second and the recorded data post-processing was performed using Matlab®.

The frequencies were extracted from each cycle of the time signals using the spectrogram function. This function, presented in Figure 7a for *inox20*, leads to time versus frequency representation. The frequency content of the spectrogram matches with the resonant frequencies because the SRTD tool was used to carry out the fatigue tests. The drop in the resonant frequency is clearly visible (in yellow). A peak is also observed on the spectrogram (see Fig. 8). It results from the resonant frequency tracking induced by the SRTD test.

The same post-processing was applied to the specimens tested to analyse the resonant frequency during the SRTD test. Since the initial resonant frequency is different for each specimen (see Tab. 3), the following normalisation equation is used to compare the results:

$$n_i(\%) = \frac{f_r^0 - f_r^i}{f_r^0} \quad (1)$$

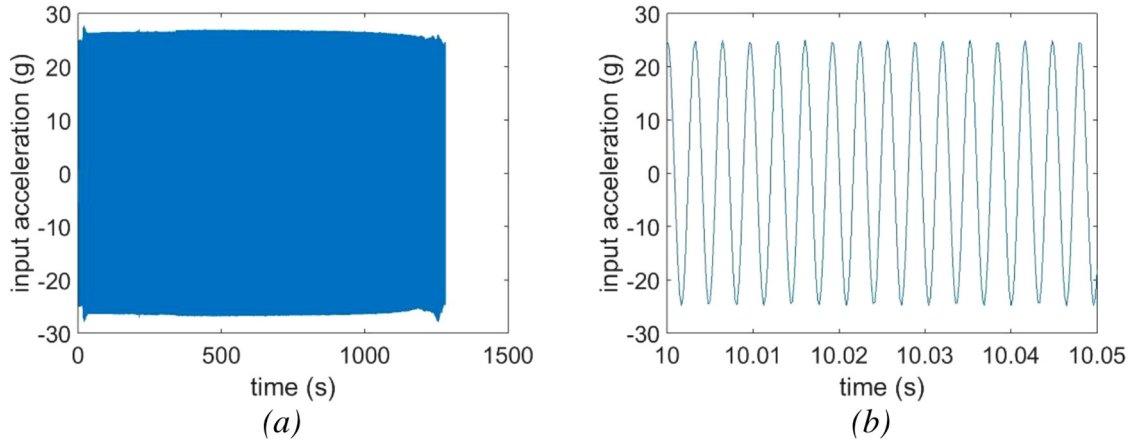

Fig. 6. A whole-time signal example (a) and a zoom on a range of this signal (b) resulting in a fatigue test.

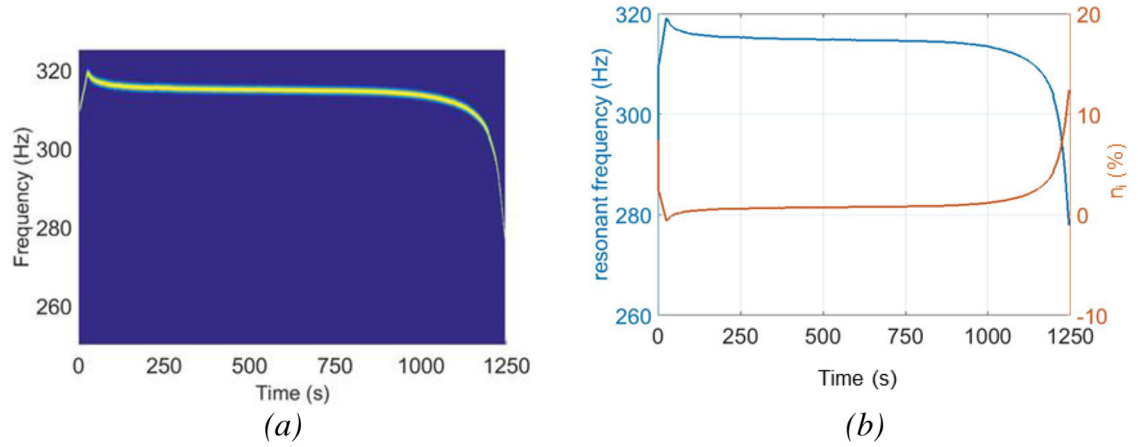

Fig. 7. Spectrogram obtained from the input acceleration (a) and diagram confronting the evolutions of the resonant frequency and the related relative deviation vs time (b).

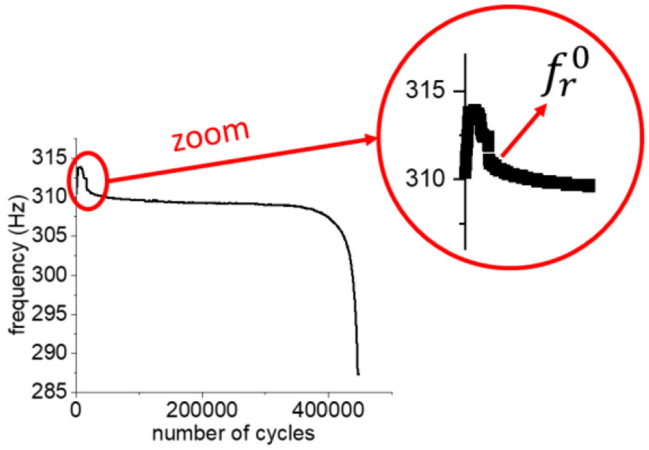

Fig. 8. Zoom on the peak due to the SRTD test on the inox16 specimen.

This parameter represents the relative deviation of the resonant frequency f_r^i with the initial resonant frequency f_r^0. The number of frequencies i extracted from the spectrogram depends on the recording time of the tests. Figure 7b confronts the evolution of n_i (%) and the resonant frequency extracted from the spectrogram. The relative deviation of the resonant frequency was widely used in the literature, mainly to define a threshold of crack initiation detection. 5% decrease in the resonant frequency was often regarded as this threshold [13–16] but, this value was also questioned by other studies [5,6,17].

Figure 9a exhibits the relative deviation of the resonant frequency during the fatigue tests of the eight specimens; the number of cycles was reached from the time and the frequency values. The statistical nature of fatigue may explain the difference observed between the numbers of cycles at failure. However, the same behaviour of the curves being observed, the number of cycles is normalised by dividing all of them by the maximum value, denoted N_f, encountered by each specimen (Fig. 9b). N_f is the number of cycles at failure, when the tests stopped because the phase error reached a value higher than 30° associated with a critical size of the crack typically over 5 mm.

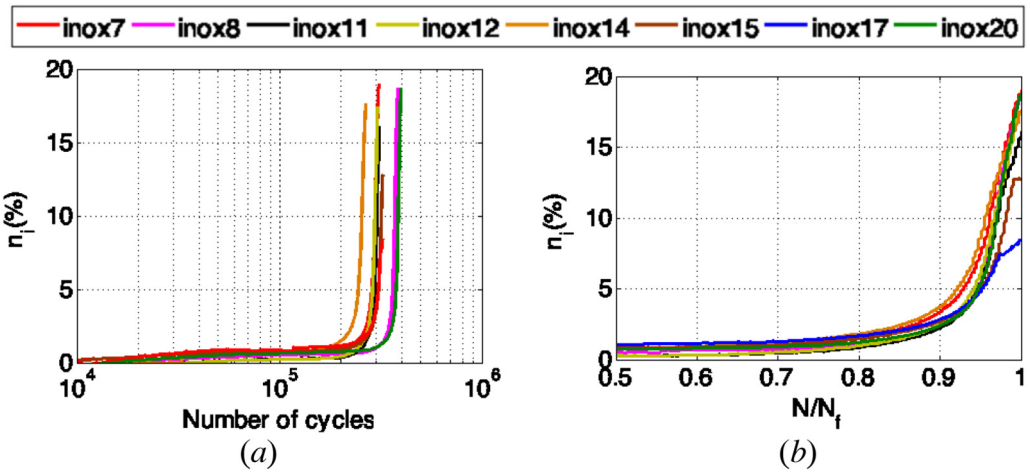

Fig. 9. Representation of the resonant frequency deviation of all the specimens during the fatigue tests (a) and the related normalisation applied to the number of cycles (b).

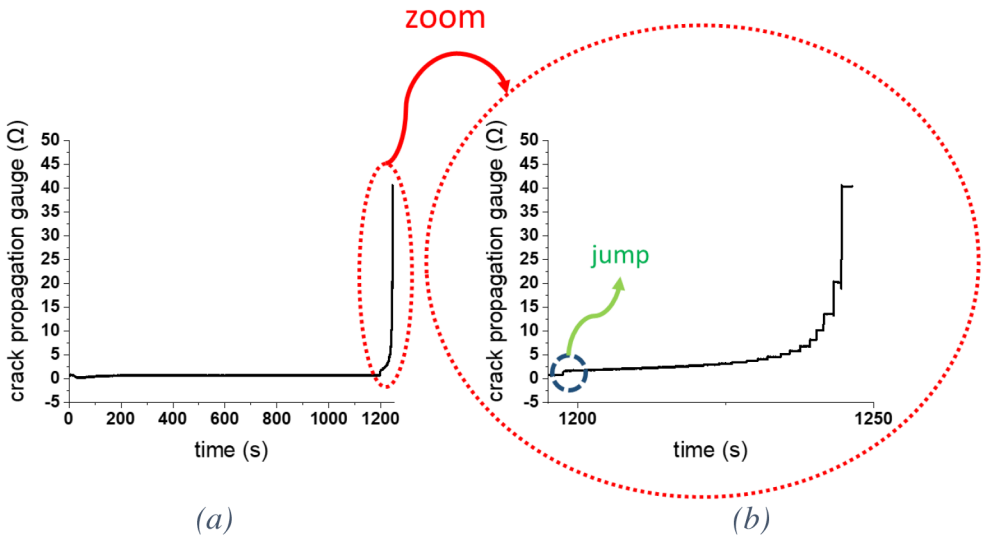

Fig. 10. The curve of the voltage signal measured on the CPG for inox20 specimen during a total test (a) and focus on a region after the jump (b).

The total lifetime of a fatigue-cracked specimen can be broken down by the number of priming and propagation cycles [7]. The curves of n_i(%) vs the number of cycles may be divided into an initial stage, propagation and final fracture stages.

The transverse crack length was obtained on the specimens showing a crack on the face equipped by CPG. Figure 10a presents the time history of the voltage signal recorded from the CPG. A jump in the voltage signal, visible in Figure 10b, was observed for all specimens. It corresponds to the crack detected by the CPG when the links are broken increasing consequently of the measured voltage. The variation in resistance of the CPG being weak at the start of the cracking stage, the acquisition system did not detect precisely this variation.

The crack length denoted a (in mm) can be deduced from the curves of the voltage signal. The minimum and maximum values are reported in Table 4. In Figure 11b, the crack length is normalised with the reduced zone width, denoted w, and the number of cycles with N_f. This figure shows that the crack has reached the second half of the reduced zone width and consumed more than 96% life. Consequently, only the last crack stage was accessible since the cracks were detected late by the CPG. It can be also observed that the behaviours of *inox7* and *inox17* are different whereas the initial strain amplitudes and resonant frequency values in Table 3 are similar. This difference can be at least partially explained by the imperfect fixture and the machining mode.

To link the results obtained from CPGs to those obtained from the resonant frequency deviation, Figure 12 is used. It shows a linear evolution between the crack length at the final stage and the resonant frequency. It is essential to quote that the final stage does not correspond to a complete fracture of the specimens; therefore, it can also be a part of the propagation stage. It is also interesting to note

Table 4. Results obtained from CPGs and resonant frequencies.

Id specimen	Minima			Maxima			$(\%)N/N_f$
	a(mm)	N	$n_i(\%)$	a(mm)	N_f	$n_i(\%)$	
Inox7	4.6	2.97E + 05	9.52	5.7	3.02E + 05	13.79	98.3
Inox8	3.6	3.61E + 05	4.16	5.7	3.73E + 05	10.85	96.8
Inox17	3.7	3.12E + 05	7.44	4.5	3.18E + 05	8.19	98.1
Inox20	3.6	3.77E + 05	4.46	5.7	3.90E + 05	12.39	96.7

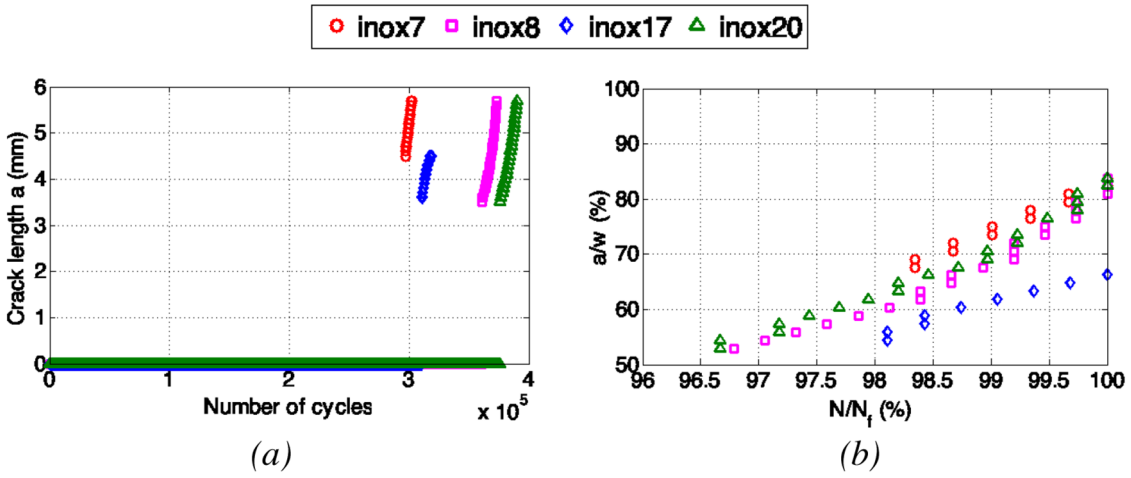

Fig. 11. (a) Crack length plotted vs the number of cycles and (b) the related normalization.

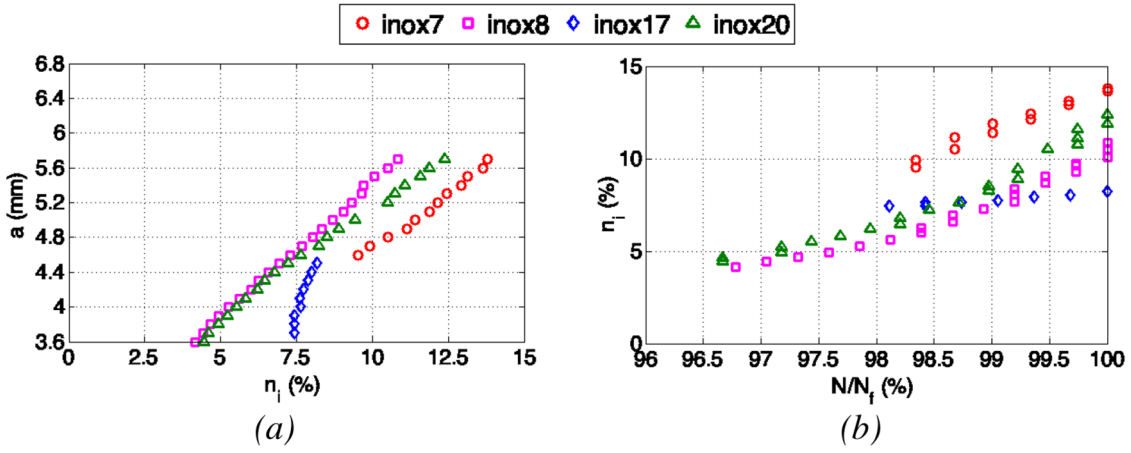

Fig. 12. Crack length vs the resonant frequency deviation.

that the trend of these curves is similar for three specimens and the crack length measured at the end of the tests are equals because of the CPG links.

Table 5 presents the results of the two specimens at 5% threshold of resonant frequency deviation. From this table, it can be emphasized that the 5% threshold used by numerous studies leads to a significant crack length and consumes approximately 97% of the portion of life.

4 Conclusion

Many vibration-fatigue tests have involved excitation with a base motion by using an electrodynamic shaker. Monitoring the crack growth in these tests is a challenge, especially to establish a failure threshold. A lot of recent studies have proposed 5% of the change in resonant frequency as this threshold. In this work, the fatigue tests

Table 5. Results obtained for $n_i \cong 5\%$.

Id specimen	a (mm)	a/w	N	$(\%)N/N_f$
Inox8	~3.9	~57.4	3.64E + 05	97.6
Inox20	~3.8	~55.9	3.79E + 05	97.2

were conducted with sine resonance track-and-dwell (SRTD) tool applied to specimens made of 304L stainless steel. This setup enables to achieve a change in the resonant frequency of the specimens when a crack appeared. Combined to the crack length measurements obtained from the CPG, the measure of the resonant frequency during the fatigue tests shows that the 5% threshold leads to a significant crack length and consumes a large portion of life. It should be recognised that for all specimens studied, the crack length in the early stages cannot be detected. This phenomenon was not observed during previous tests carried out on standard steel specimens (of similar geometry), which indicates that the reason is not technical [22]. In our opinion, this phenomenon suggests fast crack growth due to vibration [3]. Fractography study is required to identify the crack initiation sites and also to investigate any influence of test frequency on the fracture mode [23].

Furthermore, the failure threshold being essential for vibration-based bending fatigue tests, more investigations are necessary, including experiments with different reduced zone geometries and sizes.

This study was conducted within the framework of the project AMED (Multidisciplinary Analysis of Domino Effects), which has been funded with the support from the European Union with the European Regional Development Fund (ERDF) and from the Regional Council of Normandie.

References

[1] A. McGillivray, J. Hare, Offshore hydrocarbon releases 2001–2008 Health and Safety Laboratory (2008)
[2] S. Brown, E.V. Bravenec, From: ASM Failure Analysis Center, 2004: data from Handbook of Case Histories in Failure Analysis, Vol 1, K.A. Esakul, (Ed.), ASM International, 1992
[3] R. Mittal, P. Singh, D. Pukazhendi, V. Bhasin, K. Vaze, A. Ghosh, Effect of vibration loading on the fatigue life of part-through notched pipe, International Journal of Pressure Vessels and Piping **88**, 415–422 (2011)
[4] M. Mrsnik, J. Slavic, M. Boltezar, Vibration fatigue using modal decomposition, Mechanical Systems and Signal Processing **98**, 548–556 (2018)
[5] T. George, J. Seidt, M. Herman Shen, T. Nicholas, C. Cross, Development of a novel vibration-based fatigue testing methodology, International Journal of Fatigue **26**, 477–486 (2004)
[6] J. Bruns, A. Zearley, T. George, O. Scott-Emuakpor, Vibration-based bending fatigue of a hybrid insert-plate, Experimental Mechanics **55**, 1067–1080 (2015)
[7] J. Schijve, Four lectures on fatigue crack growth: I. Fatigue crack growth and fracture mechanics, Engineering Fracture Mechanics **11**, 169–181 (1979)
[8] T. Straub, Experimental investigation of crack initiation in face-centered cubic materials in the high and very high cycle fatigue regime, (2016). DOI: 10.5445/KSP/1000051515 éd.
[9] P. Lorenzino, A. Navarro, The variation of resonance frequency in fatigue tests as a tool for in-situ identification of crack initiation and propagation, and for the determination of cracked areas, International Journal of Fatigue **70**, 374–382 (2015)
[10] D. Shang, M. Barkey, Y. Wang, T. Lim, Effect of fatigue damage on the dynamic response frequency of spot-welded joints, International Journal of Fatigue **25**, 311–316 (2003)
[11] N. Giannoccaro, A. Messina, R. Nobile, F. Panella, Fatigue damage evaluation of notched specimens through resonance and anti-resonance data, Engineering Failure Analysis **13**, 340–352 (2006)
[12] R. Wang, D. Shang, L. Li, L. S., Fatigue damage model based on the natural frequency changes for spot-welded joints, International Journal of Fatigue **30**, 1047–1055 (2008)
[13] O. Salawu, Detection of structural damage through changes in frequency: a review, Engineering Structures **19**, 718–723 (1997)
[14] S. Creed, Assessment of large engineering structures using data collected during in-service loading, Structural assessment: the use of full and large scale testing, Butterworths, London, 1987
[15] W. Xu, X. Yang, B. Zhong, Y. He, C. Tao, Failure criterion of titanium alloy irregular sheet specimens for vibration-based bending fatigue testing, Engineering Fracture Mechanics **195**, 44–56 (2018)
[16] W. Xu, X. Yang, B. Zhong, G. Guo, L. Liu, C. Tao, Multiaxial fatigue investigation of titanium alloy annular discs by a vibration-based fatigue test, International Journal of Fatigue **95**, 29–37 (2017)
[17] H. Hu, Y. Li, F. Zhao, Y. Miao, P. Xue, Q. Deng, Fatigue behavior of aluminium stiffened plate subjected to random vibration loading, Transactions of Non Ferrous Metals Society of China **24**, 1331–1336 (2014)
[18] A. Collet, M. Källman, Pipe vibrations, Report 2017: 351 (2017)
[19] A. Appert, C. Gautrelet, L. Khalij, Discussion on a test bench for vibratory fatigue experiments of a cantilever beam with an electrodynamic shaker, International congress Fatigue 2018 (Poitiers), MATEC Web of Conferences **165** (2018)
[20] C. Gautrelet, L. Khalij, R. Serra, Linearity investigation from a vibratory fatigue bench, Mechanics & Industry **20**, 101 (2019)
[21] J. Minderhood, Improving SRTD Testing with resonance phase settings, Sound and Vibration **47**, 13–15 (2013)
[22] C. Gautrelet, Développement et exploitation d'un banc vibratoire en flexion pour les essais de fatigue, PHD thesis, Université Rouen Normandie/INSA Rouen Normandie, 2019
[23] C. Yan-Shin, C. Jien-Jong, The frequency effect on the fatigue crack growth rate of 304 stainless steel, Nuclear Engineering and Design **191**, 225–230 (1999)

Cite this article as: C. Gautrelet, L. Khalij, M.R. Machado, Resonance track-and-dwell testing for crack length measurement on 304L stainless steel, Mechanics & Industry **21**, 617 (2020)